Unsteady natural convection in a triangular enclosure under isothermal heating

Suvash C. Saha

School of Engineering and Physical Sciences, James Cook University,
Townsville, QLD 4811, Australia

Email: s_c_saha@yahoo.com
Tel: +61-7-4779-7523, Fax: +61-7-4781-6788

Abstract

The fluid flow and heat transfer inside a triangular enclosure due to instantaneous heating on the inclined walls are investigated using an improved scaling analysis and direct numerical simulations. The development of the unsteady natural convection boundary layer under the inclined walls may be classified into three distinct stages including a start-up stage, a transitional stage and a steady state stage, which can be clearly identified in the analytical and numerical results. A new triple-layer integral approach of scaling analysis has been considered to obtain major scaling relations of the velocity, thicknesses, Nusselt number and the flow development time of the natural convection boundary layer and verified by direct numerical simulations over a wide range of flow parameters.

KEYWORDS: Boundary layer; natural convection; scaling analysis; triangular enclosure; instantaneous heating; heating up.

Nomenclature

A	Aspect ratio of the cavity	X, Y	Dimensional coordinates
L	Length of one of the sloping walls	x, y	Dimensionless coordinates
l	Half length of the base	*Greek symbols*	
h	Vertical length of the cavity	β	Thermal expansion coefficient
g	Acceleration due to gravity	ΔT	Temperature difference between the wall and the fluid
Nu	Nusselt number	δ_T-δ_i	Dimensional viscous inner layer thickness
Nu_s	Nusselt number at steady state time	δ_{Ts} -δ_{is}	Dimensional steady state viscous inner layer thickness
P	Dimensional pressure	δ^*_T -δ^*_i	Dimensionless viscous inner layer thickness
p	Dimensionless pressure	δ^*_{Ts} -δ^*_{is}	Dimensionless steady state viscous inner layer thickness
Pr	Prandtl number	δ_T	Dimensional thermal boundary layer thickness
Ra	Rayleigh number	δ_{Ts}	Dimensional steady state thermal layer thickness
T	Temperature	δ^*_T	Dimensionless thermal boundary layer thickness
T_h	Wall temperature	δ^*_{Ts}	Dimensionless steady state thermal layer thickness
T_0	Reference temperature	δ_v	Dimensional viscous layer thickness
t	Time	δ_{vs}	Dimensional steady state viscous layer thickness
t_s	Steady state time	δ^*_v	Dimensionless viscous layer thickness
U,V	Dimensional velocity components	δ^*_{vs}	Dimensionless steady state viscous layer thickness
U_0	Reference velocity	κ	Thermal diffusivity
U_m	Dimensional velocity scale	ρ	Density
U_{ms}	Dimensional velocity scale at steady state stage	ν	Kinematic viscosity
u, v	Dimensionless velocity components	θ	Dimensionless temperature
u_m	Dimensionless velocity scale	ϕ	Angle
u_{ms}	Dimensionless velocity scale at steady state stage	τ	Dimensionless time
t_f	Dimensional heating up time	τ_s	Dimensionless steady state time
		τ_f	Dimensionless heating up time

1. Introduction

The study of natural convection in triangular enclosures is important as it has applications in many domestic and industrial systems as well as in geophysical flows. Moreover, the channels of structures, the panels of electronic apparatus and conductors in the electrical-engineering industry often have the form of a prism of triangular cross section. One important application of this type of geometry which has a great interest of many researchers recently is the natural convection through attics of buildings. The shape of many houses are isosceles triangular cross-section. One of the important objectives for design and construction of houses is to provide thermal comfort for occupants. It is also a requirement for houses to be energy efficient, i.e. the energy consumption for heating or air-conditioning houses must be minimized.

More than last three decades research relevant to the heat transfer in attics increases due to its importance in our daily life. Most of the previous research focused on the fundamental study of natural convection in attics [1–4], which is also the focus of this paper. The first reported work for this kind of geometry was conducted by Flack [5] who adopted an isosceles triangle for his experimental model and performed flow visualizations and heat transfer measurements for night-time (heating from below) conditions. It was found in his research that, at low Rayleigh numbers, the flow remained laminar. However, the flow eventually became turbulent as the Rayleigh number was increased.

Recently, an increasing number of studies have been conducted in this area [6-11]. It is revealed from the literature review that the majority of the existing research is concerned with steady-state flows and heat transfer [6,10-16]. However, a very few research have been conducted for the transient flow response [2,4,7-9]. Among these investigations, Poulikakos and Bejan [4] studied scaling analysis of the transient flow inside the attic space for the case of night-time boundary condition with the assumption that the flow is symmetric about the center plane and the aspect ratio is very small. Scaling analysis has also been performed under both heating and cooling conditions on the sloping boundaries of the attic by Saha et al. [7,8]. The numerical simulations for the transient flow response to different thermal forcing conditions have been carried out by Salmun [17] and Karyakin et al. [18]. Holtzman et al. [3] and Ridouane and Campo [4]

observed the asymmetric flow structures in an isosceles triangular enclosure due to formation of a pitchfork bifurcation for the night time cooling condition.

Asan and Namli [19] reported results for steady, laminar, two-dimensional natural convection in a pitched roof of triangular cross-section under the summer day boundary conditions. The results showed that the height-to-base ratio has a profound influence on the temperature and flow field. On the other hand, the effect of Rayleigh number is not significant for $H/B < 1$ and $Ra < 10^5$. Haese and Teubner [20] investigated the phenomenon for a large-scale triangular enclosure for night-time or winter day conditions. The authors point out that for a realistic attic space, Rayleigh numbers as high as 10^{10} or 10^{11} would be encountered. This study focused on the existing building structure.

Very recently, Saha *et al.* [21-23] have been studied scaling analysis for the transient development of the fluid flow adjacent to an inclined plate for the air ($Pr < 1$) and a range of aspect ratios and Rayleigh numbers. The authors also used those scaling results to solve the attic space problem [7-8]. Even though the scaling relations have been correctly shown the Rayleigh number (Ra) and aspect ratio (A) dependence under various flow configurations, it has also been shown that some of the scalings do not perform satisfactorily with Pr variation. This motivates us to further develop the scalings by taking into account the Pr variation in the scaling analysis. An improved scalings with Pr variation have been performed for the suddenly heated inclined flat plate by Saha *et al.* [24]. The scaling results work very well for the Pr variation of $Pr >1$. For the case of heated vertical flat plate, Lin et al [25] also have performed the improved scaling analysis with numerical verifications.

In this study suddenly imposed temperature on the sloping wall is considered and a modified triple-layer integral approach of scaling relations have been considered. The scaling results are then validated against a set of numerical results. The Prandtl number in this study is chosen greater than unity. The numerical simulations of the N-S and the energy equations have been performed for various flow parameters, Ra, Pr and A and found that the scalings work very well with numerical simulations. The heating up time scale and the time series of Nusselt number up to that time are also calculated and verified. It is found that initially the Nusselt number on the sloping wall is very high due to strong conduction effect. However, it decreases rapidly up to the steady state time of

the boundary layer. Then it reduces again when the whole cavity becomes heated up. The scaling results derived here may be useful for the builder for their air-conditioning calculation.

2. Problem formulation

Under consideration is the unsteady flow behaviour resulting from heating a quiescent, isothermal Newtonian fluid with $Pr > 1$ in a two-dimensional triangular cavity of height h and horizontal length $2l$ by imposing a fixed higher temperature, T_h, on both inclined walls, as shown in Fig. 1. The fluid is initially at rest and at a uniform temperature T_0 ($T_0 < T_h$). The bottom surface is kept adiabatic and all boundaries are nonslip. It is also assumed that the flow is laminar. In order to avoid the singularities at the tips in the numerical simulation, the tips are cut off by 5% and at the cutting points (refer to Figure 1) rigid non-slip and adiabatic vertical walls are assumed. We anticipate that this modification of the geometry will not alter the overall flow development significantly.

The development of the flow under the inclined plate is governed by the following two-dimensional Navier–Stokes and energy equation with the Boussinesq approximation:

$$\frac{\partial U}{\partial X} + \frac{\partial V}{\partial Y} = 0 \tag{1}$$

$$\frac{\partial U}{\partial t} + U\frac{\partial U}{\partial X} + V\frac{\partial U}{\partial Y} = -\frac{1}{\rho}\frac{\partial P}{\partial X} + \nu\left(\frac{\partial^2 U}{\partial X^2} + \frac{\partial^2 U}{\partial Y^2}\right) + g\sin\phi\beta\left(T - T_0\right) \tag{2}$$

$$\frac{\partial V}{\partial t} + U\frac{\partial V}{\partial X} + V\frac{\partial V}{\partial Y} = -\frac{1}{\rho}\frac{\partial P}{\partial Y} + \nu\left(\frac{\partial^2 V}{\partial X^2} + \frac{\partial^2 V}{\partial Y^2}\right) + g\cos\phi\beta\left(T - T_0\right) \tag{3}$$

$$\frac{\partial T}{\partial t} + U\frac{\partial T}{\partial X} + V\frac{\partial T}{\partial Y} = \kappa\left(\frac{\partial^2 T}{\partial X^2} + \frac{\partial^2 T}{\partial Y^2}\right) \tag{4}$$

The initial and boundary conditions are defined as follows:

- On the sloping walls a rigid non-slip wall and a constant temperature condition, $T = T_h$ are applied.

- The bottom horizontal wall is adiabatic ($\partial T/\partial n$ = 0, where n is the direction normal to the wall) and rigid non-slip.
- At the cutting points of the bottom tips, rigid non-slip and adiabatic vertical walls are assumed.
- Initially the fluid is quiescent and isothermal at temperature T_0.

The flow development is determined by three governing parameters: the Rayleigh number (Ra), the Prandtl number (Pr) and the slope (A). They are defined respectively as follows,

$$Ra = \frac{g\beta\Delta T h^3}{\kappa\nu}, \quad \mathrm{Pr} = \frac{\nu}{\kappa}, \quad A = \frac{h}{l} \tag{5}$$

A typical flow development of the boundary layer is illustrated in figure 2, where numerically simulated temperature contours and the streamlines are shown for the specific case of $Ra = 10^7$, $Pr = 10$ and $A = 0.5$.

3. Scaling Analysis

As soon as the sloping walls are heated, a boundary layer starts to grow adjacent to the walls. The flow can be classified into several stages of the boundary layer development. A start-up stage is dominated by conduction which is normal to the inclined wall, followed by a short transitional stage with some overshoots and undershoots before reaching a steady-state stage. However, hot fluid thorough the boundary layer ejected from the top of the cavity into the core and eventually heated up the entire domain. The parameters characterise the flow behaviour at the boundary-layer development stage: δ_T, the thermal boundary layer thickness, U_m, the maximum velocity parallel to the inclined walls within the boundary layer, t_s, the time for the boundary layer to reach the steady state, t_f, the time for the whole cavity to become heated up, Nu_s, the steady state Nusselt number. The present scaling analysis is the modification of the scaling derived by [8]. To show the effect of the Prandtl number on the boundary layer it is necessary to examine the structure of the boundary layer in more detail.

3.1 Start up stage

Since initially the fluid is quiescent and uniform in the domain, the energy equation (3) indicates that heat from the plate will transfer into the fluid layer through conduction, resulting in a thermal boundary layer of thickness δ_T. This is because the advection term ($U\Delta T/h$) in the energy equation (3) is much smaller than the conduction term for a very small time. The dominant balance is between the unsteady and conduction terms, that is,

$$\frac{\Delta T}{t} \sim \kappa \frac{\Delta T}{\delta_T^2} \Rightarrow \delta_T \sim \kappa^{1/2} t^{1/2} \tag{6}$$

This scaling is valid until the convection term becomes important.

The unsteady inertia, viscous and advection terms of the momentum equation (2) are $O(U/t)$, $O(\nu U/\delta_T^2)$ and $O(U^2/L)$ respectively. The ratio of the advection term to the unsteady term is $O(Ut/L)$. For sufficiently small time, this ratio is much smaller and thus the advection term is not significant. In addition, the ratio of the unsteady to viscous term is $(U/t)/(\nu U/\delta_T^2) \sim 1/Pr$, where $Pr = \nu/\kappa$. For $Pr >> 1$, the unsteady term is also smaller than the viscous term and thus the correct balance is between the viscosity and the buoyancy in the momentum equation (2).

$$0 \sim \nu \frac{\partial^2 U}{\partial Y^2} + g\beta\Delta T \sin\phi \tag{7}$$

Figure 3 shows the profiles of the temperature and velocity along a line perpendicular to the left inclined wall of the enclosure at its mid point. Since the momentum boundary condition of the wall is no-slip, the velocity of the fluid is zero at the surface. The velocity increases from zero at the inclined wall and reaches its maximum which occurs within δ_T. The velocity then decreases as the position is further from the wall. The validation of the scaling relations of the flow features will be shown in the following section. It is worth noting that for $Pr < 1$ the scenario is different, which is out of scope of this study. Outside the thermal layer the balance between viscosity and buoyancy is invalid. Instead, the fluid is driven by the diffusion of momentum by viscosity from the region accelerated by buoyancy. The viscous layer thickness is defined by the length

scale δ_v. Therefore, we may divide the whole boundary layer into three regions as shown in figure 3.

In regions I and II, the balance is between the viscosity and the buoyancy. However, in region III the balance is between viscosity and inertia. In region I (the inner viscous layer), the balance (7) gives:

$$U_m \sim \frac{g\beta\Delta T \sin\phi}{\nu}(\delta_T - \delta_i)^2 \tag{8}$$

In region II, the limit of the integral is taken between (δ_T- δ_i) and δ_T.

$$0 \sim \left[\nu \frac{\partial U}{\partial Y}\right]_{\delta_T-\delta_i}^{\delta_T} + g\beta \sin\phi \int_{\delta_T-\delta_i}^{\delta_T} T dY \tag{9}$$

Note that $\partial U/\partial Y = 0$ at δT-δi since the velocity is maximum there. Additionally, we have

$$\left[\frac{\partial U}{\partial Y}\right]_{\delta_T} \sim \frac{U_m}{\delta_v - \delta_T + \delta_i} \text{ and } \int_{\delta_T-\delta_i}^{\delta_T} T dY \sim \Delta T \delta_i \tag{10}$$

Hence, (8) becomes,

$$U_m \sim \frac{g\beta\Delta T \sin\phi}{\nu}\delta_i(\delta_v - \delta_T + \delta_i) \tag{11}$$

Equating (11) to (8), we may obtain

$$\delta_i \sim \frac{\delta_T^2}{\delta_T + \delta_v} \tag{12}$$

As the buoyancy force is negligible in region III, the flow is driven solely by diffusion of momentum in which the unsteady term balances the viscous term, yielding

$$\frac{U_m}{t} \sim \nu \frac{U_m}{\delta_v^2} \tag{13}$$

and further

$$\delta_v \sim \nu^{1/2} t^{1/2} \sim \mathrm{Pr}^{1/2}\, \delta_T \tag{14}$$

Hence, (12) becomes,

$$\delta_i \sim \frac{\kappa^{1/2} t^{1/2}}{1 + \mathrm{Pr}^{1/2}} \tag{15}$$

Additionally, the length of the inner viscous layer (region I) is

$$\delta_T - \delta_i \sim \delta_T - \frac{\delta_T}{1+\mathrm{Pr}^{1/2}} \sim \frac{\kappa^{1/2} t^{1/2}}{1+\mathrm{Pr}^{-1/2}} \tag{16}$$

Inserting (6) and (15) into (8), we obtain

$$U_m \sim \frac{g \sin\phi \beta \Delta T}{\nu} \left(\frac{\mathrm{Pr}}{1+\mathrm{Pr}^{1/2}} \right)^2 \kappa t \sim \frac{Ra \kappa^2 A}{h^3 \left(1+A^2\right)^{1/2}} \left(\frac{1}{1+\mathrm{Pr}^{-1/2}} \right)^2 t \tag{17}$$

(17) is the scaling for U_m at the start-up stage

The local Nusselt number at any x on the inclined plate at the start-up stage is

$$Nu \sim \frac{\partial T / \partial Y\big|_{Y=0}}{\Delta T / h} \sim \frac{h}{\Delta T} \frac{\Delta T}{\delta_T} \sim \frac{h}{\kappa^{1/2} t^{1/2}} \tag{18}$$

and the global Nusslet number at the start-up stage is

$$Nu \sim \frac{1}{L} \int_0^L Nu dx \tag{19}$$

3.2 Steady state stage:

As time increases the more heat is convected away. The boundary layer approaches a steady state until convection balances conduction, i.e.

$$U_m \frac{\Delta T}{L} \sim \kappa \frac{\Delta T}{\delta_T^2} \tag{20}$$

which leads to a time scale when the boundary layer reaches a steady state,

$$t_s \sim \frac{h^2}{Ra^{1/2} \kappa} \frac{\left(1+A^2\right)^{1/2}}{A} \left(1+\mathrm{Pr}^{-1/2}\right) \tag{21}$$

The corresponding maximum velocity scale at the steady state time is

$$U_{ms} \sim \frac{Ra^{1/2} \kappa}{h} \frac{1}{\left(1+\mathrm{Pr}^{-1/2}\right)} \tag{22}$$

The steady-state thickness scale of the thermal boundary layer is

$$\delta_{Ts} \sim \frac{h}{Ra^{1/4}} \frac{\left(1+A^2\right)^{1/4}}{A^{1/2}} \left(1+\mathrm{Pr}^{-1/2}\right)^{1/2} \tag{23}$$

The scaling of the steady state inner viscous boundary layer thickness is

$$\delta_{Ts} - \delta_{is} \sim \frac{h}{Ra^{1/4}} \frac{\left(1+A^2\right)^{1/4}}{A^{1/2}} \frac{1}{\left(1+\mathrm{Pr}^{-1/2}\right)^{1/2}} \tag{24}$$

The scaling of the steady state viscous boundary layer thickness is

$$\delta_{vs} \sim \mathrm{Pr}^{1/2}\, \delta_{Ts} \sim \frac{h}{Ra^{1/4}} \frac{\left(1+A^2\right)^{1/4}}{A^{1/2}} \mathrm{Pr}^{1/2} \left(1+\mathrm{Pr}^{-1/2}\right)^{1/2} \tag{25}$$

At a steady state, the global Nusselt number is:

$$Nu_s \sim \frac{A^{1/2} Ra^{1/4}}{\left(1+A^2\right)^{1/4}} \frac{1}{\left(1+\mathrm{Pr}^{-1/2}\right)^{1/2}} \tag{26}$$

Heating up stage:

Once the boundary layer is fully developed, The hot fluid through the boundary layer from both sloping walls meet on the top tip of the cavity. Then it has no choice but to move downward. This way the interior of the enclosure is gradually stratified, starting from the top of the cavity, and this heating-up stage continues until the hot fluid layer from the top reaches the bottom surface. The appropriate parameters to characterize this heating-up stage are the time, t_f for the fluid to be fully heated-up and the average Nusselt number on the heated wall.

During the heating-up stage, let us consider an arbitrary moment, *t*. At this moment, the fluid inside the enclosure can be assumed to consist of two layers with the location $x = x_i$ as the interface. The bottom layer is at the original temperature, T_0 whereas the top layer is filled with the hot fluid discharged from the thermal boundary layer, the temperature of which is assumed to be the same as the wall temperature T_h.

From ΔMNO and ΔMPQ in Figure 4, we have,

$$\frac{L-x_i}{L} = \frac{h-h_i}{h} \Rightarrow h - h_i = h\left(1 - \frac{x_i}{L}\right), \tag{27}$$

and

$$\frac{L}{L-x_i} = \frac{l}{PQ} \Rightarrow PQ = l\left(1 - \frac{x_i}{L}\right) \tag{28}$$

Therefore

$$\Delta MPQ = \frac{1}{2} hl\left(1-\frac{x_i}{L}\right)^2 \sim \frac{h^2}{A}\left(1-\frac{x_i}{L}\right)^2 \tag{29}$$

Suppose the total volume of the enclosure ABC is

$$V_w = \frac{1}{2} lh\,. \tag{30}$$

At the steady state time the volume filled by the hot fluid is

$$V_s \sim U_{ms}\delta_{Ts} t_s\,, \tag{31}$$

which gives

$$V_s \sim \frac{h^2\left(1+\mathrm{Pr}^{-1/2}\right)^{1/2}\left(1+A^2\right)^{3/4}}{Ra^{1/4}A^{3/2}}, \tag{32}$$

The ratio of the volumes

$$\frac{V_s}{V_w} \sim \frac{\left(1+\mathrm{Pr}^{-1/2}\right)^{1/2}\left(1+A^2\right)^{3/4}}{Ra^{1/4}A^{1/2}} \tag{33}$$

It is estimated that the maximum ratio of the volume filled by hot fluid during the transient stage (from start-up to the steady state time) to the total volume of the enclosure is less than 0.095 over the ranges of *Ra*, *Pr*, *A* and other parameters considered here. Therefore, the filled volume at the transient stage is insignificant compared to the total volume and is neglected below.

From the mass conservation law

$$\frac{h^2}{A}\left(1-\frac{x_i}{L}\right)^2 \sim U_{ms}\delta_{Ts} t \tag{34}$$

Now applying (22) and (23) in (34) we have,

$$x_i \sim L\left[1-\frac{A^{1/4}Ra^{1/8}\kappa^{1/2}\left(1+A^2\right)^{1/8}}{h\left(1+\mathrm{Pr}^{-1/2}\right)^{1/4}} t^{1/2}\right] \tag{35}$$

The time when the whole enclosure is filled with hot fluid ($x_i \sim 0$) is obtained as

$$t_f \sim \frac{h^2\left(1+\mathrm{Pr}^{-1/2}\right)^{1/2}}{A^{1/2}Ra^{1/4}\kappa\left(1+A^2\right)^{1/4}} \tag{36}$$

Since only the lower part of the sloping wall contributes to the heat transfer at any given time, it is apparent from (26) that the global Nusselt number, *Nu* at the heating up stage is,

$$Nu \sim \left(\frac{x_i}{L}\right) Nu_s. \tag{37}$$

Applying (35) and (36) in (37), we have

$$\frac{Nu}{Nu_s} \sim \left[1 - \frac{A^{1/4} Ra^{1/8} \kappa^{1/2} \left(1 + A^2\right)^{1/8}}{h\left(1 + \mathrm{Pr}^{-1/2}\right)^{1/4}} t^{1/2}\right]$$

$$\Rightarrow \frac{Nu}{Nu_s} \sim 1 - \left(\frac{t}{t_f}\right)^{1/2}. \tag{38}$$

4. Normalization of the governing equations and the scaling:

To verify the various scales, numerical solution of the full Navier-stokes equations and the energy equation are obtained for a range of *Ra*, *Pr* and *A* values. For convenience, the non- dimensionalised forms of the governing equations are adopted

$$\frac{\partial u}{\partial x} + \frac{\partial v}{\partial y} = 0 \tag{39}$$

$$\frac{\partial u}{\partial \tau} + u\frac{\partial u}{\partial x} + v\frac{\partial u}{\partial y} = -\frac{\partial p}{\partial x} + \frac{\mathrm{Pr}}{Ra^{1/2}}\left(\frac{\partial^2 u}{\partial x^2} + \frac{\partial^2 u}{\partial y^2}\right) + \mathrm{Pr}\,\theta \sin\phi \tag{40}$$

$$\frac{\partial v}{\partial \tau} + u\frac{\partial v}{\partial x} + v\frac{\partial u}{\partial y} = -\frac{\partial p}{\partial y} + \frac{\mathrm{Pr}}{Ra^{1/2}}\left(\frac{\partial^2 v}{\partial x^2} + \frac{\partial^2 v}{\partial y^2}\right) + \mathrm{Pr}\,\theta \cos\phi \tag{41}$$

$$\frac{\partial \theta}{\partial \tau} + u\frac{\partial \theta}{\partial x} + v\frac{\partial \theta}{\partial y} = \frac{1}{Ra^{1/2}}\left(\frac{\partial^2 \theta}{\partial x^2} + \frac{\partial^2 \theta}{\partial y^2}\right) \tag{42}$$

where *x*, *y*, *u*, *v*, θ, *p* and τ are the normalised forms of *X*, *Y*, *U*, *V*, *T*, *P* and *t*, respectively, which are made normalised by the following set of expressions:

$$x = \frac{X}{h}, \quad y = \frac{Y}{h}, \quad u = \frac{U}{U_0}, \quad v = \frac{V}{U_0}, \quad \tau = \frac{t}{h/U_0}$$
$$p = \frac{P}{\rho U_0^2}, \quad \theta = \frac{T - T_0}{T_w - T_0} \tag{43}$$

where $U_0 = \kappa Ra^{1/2}/h$. The origin of the coordinate system is located at the leading edge of the heated plate.

The scaling relations obtained above are normalised as follows:

$$\delta_T^* = \frac{\delta_T}{h} \sim \frac{\tau^{1/2}}{Ra^{1/4}} \tag{44}$$

$$\delta_v^* = \frac{\delta_v}{h} \sim \frac{\mathrm{Pr}^{1/2}\,\tau^{1/2}}{Ra^{1/4}} \tag{45}$$

$$\delta_T^* - \delta_i^* = \frac{\delta_T - \delta_i}{h} \sim \frac{1}{1+\mathrm{Pr}^{-1/2}} \frac{\tau^{1/2}}{Ra^{1/4}} \tag{46}$$

and

$$u_m = \frac{U_m}{U_0} \sim \frac{A}{\left(1+A^2\right)^{1/2}} \frac{\tau}{\left(1+\mathrm{Pr}^{-1/2}\right)^2} \tag{47}$$

The dimensionless form of (22) at a steady state time is

$$\tau_s = \frac{t_s}{h/U_0} \sim \frac{\left(1+A^2\right)^{1/2}}{A}\left(1+\mathrm{Pr}^{-1/2}\right) \tag{48}$$

At the steady state, (23), (24), (25) and (26) are re-written in the dimensionless form:

$$u_{ms} = \frac{U_{ms}}{U_0} \sim \frac{1}{1+\mathrm{Pr}^{-1/2}} \tag{49}$$

$$\delta_{Ts}^* = \frac{\delta_{Ts}}{h} \sim \frac{\left(1+A^2\right)^{1/4}}{Ra^{1/4}A^{1/2}}\left(1+\mathrm{Pr}^{-1/2}\right)^{1/2} \tag{50}$$

$$\delta_{Ts}^* - \delta_{is}^* = \frac{\delta_{vis}}{h} \sim \frac{\left(1+A^2\right)^{1/4}}{Ra^{1/4}A^{1/2}} \frac{1}{\left(1+\mathrm{Pr}^{-1/2}\right)^{1/2}} \tag{51}$$

$$\delta_{vs}^* = \frac{\delta_{vs}}{h} \sim \frac{\left(1+A^2\right)^{1/4}}{Ra^{1/4}A^{1/2}}\mathrm{Pr}^{1/2}\left(1+\mathrm{Pr}^{-1/2}\right)^{1/2} \tag{52}$$

At the heating up time, (36) and (38) are normalised respectively as

$$\tau_f \sim \frac{Ra^{1/4}\left(1+\mathrm{Pr}^{-1/2}\right)^{1/2}}{A^{1/2}\left(1+A^2\right)^{1/4}} \tag{53}$$

$$\frac{Nu}{Nu_s} = 1-\left(\frac{\tau}{\tau_f}\right)^{1/2} \tag{54}$$

5. Numerical procedure

Equations (1) - (4) are solved along with the initial and boundary conditions using the SIMPLE scheme. The Finite Volume scheme has been chosen to discretize the governing equations, with the QUICK scheme (see Leonard and Mokhtari [26]) approximating the advection term. The diffusion terms are discretized using central-differencing with second order accurate. A second order implicit time-marching scheme has also been used for the unsteady term. The detailed numerical procedure can be found in [7-9].

6. Results and discussions

The flow features discussed theoretically above are verified on the basis of a complete series of numerical simulations. It is assumed that the fluid contained in the attic space is originally quiescent and of a uniform temperature θ = 0. A sudden heating boundary condition is applied on the sloping walls of the cavity. Throughout this simulation, the horizontal bottom wall is assumed to be adiabatic. The above scales have been developed with an assumption that the flow is symmetric along the symmetry center line of the cavity. Previous studies of attic space have revealed that the flow is indeed symmetric along the center line for the case of heating on the sloping walls.

The detailed validation of the boundary layer development has been discussed in Saha, et al. [24] (e.g. velocity scale, thickness scale etc). For brevity, those results are not repeated here. However, heat transfer scales together with steady state time scales have been verified in this study. Moreover, the heating-up time scale and the subsequent heat transfer scale at that time have also been verified.

The heating-up time is determined by the heat flux through the natural convection boundary layer. The hot fluid moves upward along the boundary layers of both inclined walls and meets under the apex of the enclosure. Then it has no choice but to move downward right below the tip, forming a horizontal stratification. This stratified hot fluid fills the enclosure, ultimately reaching the bottom surface at which time the whole enclosure is filled with hot fluid.

Table 1 shows all simulation cases in this study in which Runs 1-5 with Pr = 5, 10, 20, 50 and 100 while keeping A = 0.5 and Ra = 1.0×10^7 unchanged are carried out to show the dependence of the scaling relations on the Prandtl number; Runs 6-9 and 2 with Ra = 1.0×10^6, 5.0×10^6, 5.0×10^7, 1.0×10^8 and 1.0×10^7 while keeping Pr = 10 and A = 0.5 unchanged to show the dependence on the Rayleigh number; and Runs 10-11 and 2 with A = 1.0, 0.2 and 0.5 while keeping Pr = 10 and Ra = 1.0×10^7 unchanged to show the dependence of the slope of the inclination of the plate.

The numerical results showing the dependence of the instantaneous average Nusselt number Nu on Ra, Pr and A at the boundary-layer development stage and at the heating-up stage are presented in Figure 5 and 6. Figure 5(a) shows the raw data of the time series of the Nusselt number which have been calculated on the left inclined wall of the cavity for different Rayleigh numbers, Prandtl numbers and aspect ratios. It is found that the Nusselt number depends strongly on Ra, Pr and A. It is also noticed that initially Nusselt number for different parameters are very high due to strong conduction effect. Then it decreases gradually and become steady state. However, the return flow from the top eventually occupied the entire cavity which affects the Nusselt numbers. The Nusselt number approaches zero when the whole cavity becomes heated up. In Figure 5(b), the time has been normalized with respect to the steady state time, $(1+A^2)^{1/2}(1+Pr^{-1/2})/A$, of the boundary layer development. We notice that the steady state of the Nusselt numbers fall on a vertical line (long dashed line), which validates the steady state time scale of the boundary layer development (48).

The Nusselt number is now normalized with respect to its steady state value, $A^{1/2}Ra^{1/4}/[(1+A^2)^{1/4}(1+Pr^{-1/2})^{1/2}]$ and plotted against normalized time with respect to the steady state time scale in Figure 6(a). As anticipated, all lines collapse together in one line up to the steady state time. This validates the scaling relation (26) together with the

time scale (48) at the boundary-layer development stage. Finally, the normalized Nusselt number has been plotted against $1-(\tau/\tau_f)^{1/2}$ in Figure 6(b). Again all lines collapse on a single line which validates the scaling relation (54) at the heating up stage. Note that the x-axis is on a log scale of figure 6(b).

To verify the heating-up time scale, the temperature has been recorded at the midpoint of the bottom surface, which is shown in Figure 7. Raw data of the time series of the temperature for different Rayleigh numbers, Prandtl numbers and aspect ratios are plotted in Figure 7(a). It is anticipated that initially there is no response of the temperature at the middle point of the bottom surface. The hot fluid from the boundary layer discharge from the top and the enclosure gradually becomes stratified from the top. As soon as the hot fluid reaches the bottom, the temperature starts to increase. However, this response time is different for different Ra, Pr and A. In Figure 7(b), the time is normalized with respect to the heating-up time, $\tau_f \sim Ra^{1/4}(1+Pr^{-1/2})^{1/2}/[A^{1/2}(1+A^2)^{1/4}]$ and the temperature has been normalized by the temperature difference. We see that the temperature series response at the same time for different flow parameters. This confirms that the heating-up time scale (53) is accurate.

7 Conclusions

Natural convection under a heated triangular cavity is examined by modified scaling analysis and verified by numerical simulations for various parameters considered here. The verification of the scaling relations includes steady state time scale of the boundary-layer development as well as the heat transfer rate. Moreover, heating up time scale and the Nusselt number at that time are also verified by numerical simulations. Numerical results demonstrate that the scaling relations are able to accurately characterize the physical behaviour in each stage of the flow development, including the start-up stage, the transitional stage, the steady state stage and the heating up stage. The present scaling analysis incorporates a detailed balance in the momentum equation depending on the thickness of the boundary layer that improves scaling predictions especially where the Pr variation effect is taken into account. The scaling relations are formed based on the established characteristic flow parameters of the maximum velocity in the boundary layer

(u_m), the time for the boundary layer to reach the steady state (t_s) and the thermal (δ_T) and viscous (δ_v) boundary layer thickness. Through comparisons of the scaling relations with the numerical simulations, it is found that the scaling results agree well with the numerical simulations.

Acknowledgements:

The author gratefully acknowledges to the comments and suggestions of the anonymous reviewers to improve this paper.

References

[1] D. Poulikakos, A. Bejan, Natural convection experiments in a triangular enclosure, J. Heat Transfer, Trans. ASME 105 (1983) 652–655.

[2] D. Poulikakos, A. Bejan, The fluid dynamics of an attic space, J. Fluid Mech. 131 (1983) 251–269.

[3] G.A. Holtzman, R.W. Hill, K.S. Ball, Laminar natural convection in isosceles triangular enclosures heated from below and symmetrically cooled from above, J. Heat Transfer, Trans. ASME 122 (2000) 485–491.

[4] E.H. Ridouane, A. Campo, Formation of a pitchfork bifurcation in thermal convection flow inside an isosceles triangular cavity, Phys. Fluids 18 (2006) 074102.

[5] R.D. Flack, The experimental measurement of natural convection heat transfer in triangular enclosures heated or cooled from bellow. ASME Journal of Heat Transfer 102 (1980) 770-772.

[6] E. F. Kent, Numerical analysis of laminar natural convection in isosceles triangular enclosures for cold base and hot inclined walls, Mechanics Research Communications 36 (2009) 497–508.

[7] S. C. Saha, J. C. Patterson, C. Lei, Natural convection in attics subject to instantaneous and ramp cooling boundary conditions, Energy and Buildings, 42 (2010) 1192-1204.

[8] S. C. Saha, J. C. Patterson, C. Lei, Natural convection in attic-shaped spaces subject to sudden and ramp heating boundary conditions, Heat and Mass Transfer 46 (2010)

621-638.

[9] S. C. Saha, J. C. Patterson, C. Lei, Natural convection and heat transfer in attics subject to periodic thermal forcing, International Journal of Thermal Sciences 49 (2010) 1899-1910.

[10] H.F. Oztop, Y. Varol, A. Koca, Laminar natural convection heat transfer in a shed roof with or without eave for summer season, Appl. Therm. Eng. 27 (2007) 2252–2265.

[11] A.Koca, H.F. Oztop, Y. Varol, The effects of Prandtl number on natural convection in triangular enclosures with localized heating from below, Int. Commun. Heat Mass Transfer 34 (2007) 511–518.

[12] V.A. Akinsete, T.A. Coleman, Heat transfer by steady laminar free convection in triangular enclosures, Int. J. Heat Mass Transfer 25 (7) (1982) 991–998.

[13] S.C. Tzeng, J.H. Liou, R.Y. Jou, Numerical simulation-aided parametric analysis of natural convection in a roof of triangular enclosures, Heat Transfer Eng. 26 (8) (2005) 69–79.

[14] E.H. Ridouane, A. Campo, M. McGarry, Numerical computation of buoyant airflows confined to attic spaces under opposing hot and cold wall conditions, Int. J. Therm. Sci. 44 (10) (2005) 944–952.

[15] E.M. del Campo, M. Sen, E. Ramos, Analysis of laminar natural convection in a triangular enclosure, Numer. Heat Transfer 13 (1988) 353–372.

[16] H. Asan, L. Namli, Numerical simulation of buoyant flow in a roof of triangular cross-section under winter day boundary conditions, Energy and Buildings 33 (7) (2001) 753–757.

[17] H. Salmun, Convection patterns in a triangular domain, Int. J. Heat Mass Transfer 38 (2) (1995) 351–362.

[18] Y.E. Karyakin, Y.A. Sokovishin, O.G. Martynenko, Transient natural convection in triangular enclosures, Int. J. Heat Mass Transfer 31 (9) (1988) 1759–1766.

[19] H. Asan, L. Namli, Laminar natural convection in a pitched roof of triangular cross-section: summer day boundary conditions, Energy and Buildings 33 (2000) 69–73.

[20] P.M. Haese, M.D. Teubner, Heat exchange in an attic space, Int. J. Heat Mass Transfer 45 (2002) 4925–4936.

[21] S. C. Saha, J. C. Patterson, C. Lei, Natural convection boundary layer adjacent to an inclined flat plate subject to sudden and ramp heating, International Journal of Thermal Sciences, 49 (2010) 1600-1612.

[22] S. C. Saha, J. C. Patterson, C. Lei, "Scaling of natural convection of an inclined flat plate: Ramp cooling condition", *International Journal of Heat and Mass Transfer*, (*In Press*), 10.1016/j.ijheatmasstransfer.2010.07.047, 2010.

[23] S. C. Saha, J. C. Patterson, C. Lei, Scaling of natural convection of an inclined flat plate: Sudden cooling condition, Trans. ASME Journal of Heat Transfer. (*Accepted*), 2010.

[24] S. C. Saha, F. Xu, M. M. Molla, "Scaling analysis of the unsteady natural convection boundary layer adjacent to an inclined plate for $Pr > 1$ following instantaneous heating", Submitted to *ASME Journal of Heat Transfer*.

[25] W. Lin, S.W. Armfield, J.C. Patterson, C. Lei, Prandtl number scaling of unsteady natural convection boundary layers of $Pr > 1$ fluids under isothermal heating, Phys. Rev. E, 79 (2009) 066313.

[26] B.P. Leonard, S. Mokhtari, ULTRA-SHARP Nonoscillatory Convection Schemes for High-Speed Steady Multidimensional Flow, NASA TM 1-2568 (ICOMP-90-12), NASA Lewis Research Centre (1990).

Table 1
Values of *Ra*, *Pr* and *A* for 11 simulations run

Run number	***Ra***	***Pr***	***A***
1	1.0×10^{7}	5	0.5
2	1.0×10^{7}	10	0.5
3	1.0×10^{7}	20	0.5
4	1.0×10^{7}	50	0.5
5	1.0×10^{7}	100	0.5
6	1.0×10^{6}	10	0.5
7	5.0×10^{6}	10	0.5
8	5.0×10^{7}	10	0.5
9	1.0×10^{8}	10	0.5
10	1.0×10^{7}	10	1.0
11	1.0×10^{7}	10	0.2

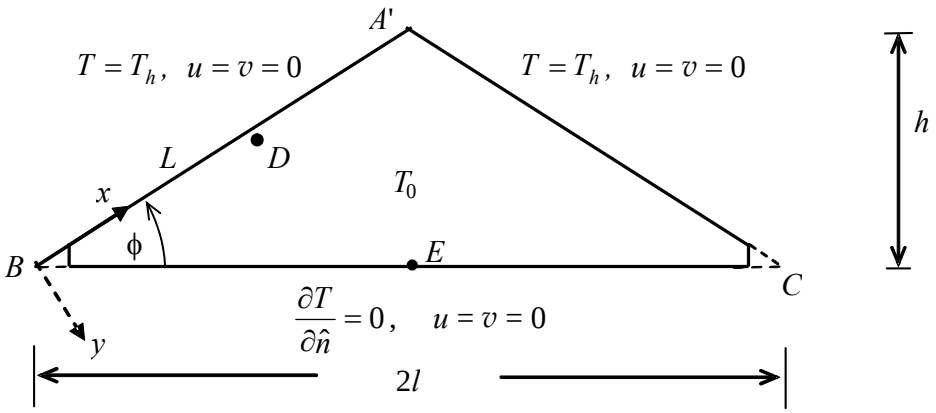

Fig.1. Schematic of the computational domain and boundary conditions.

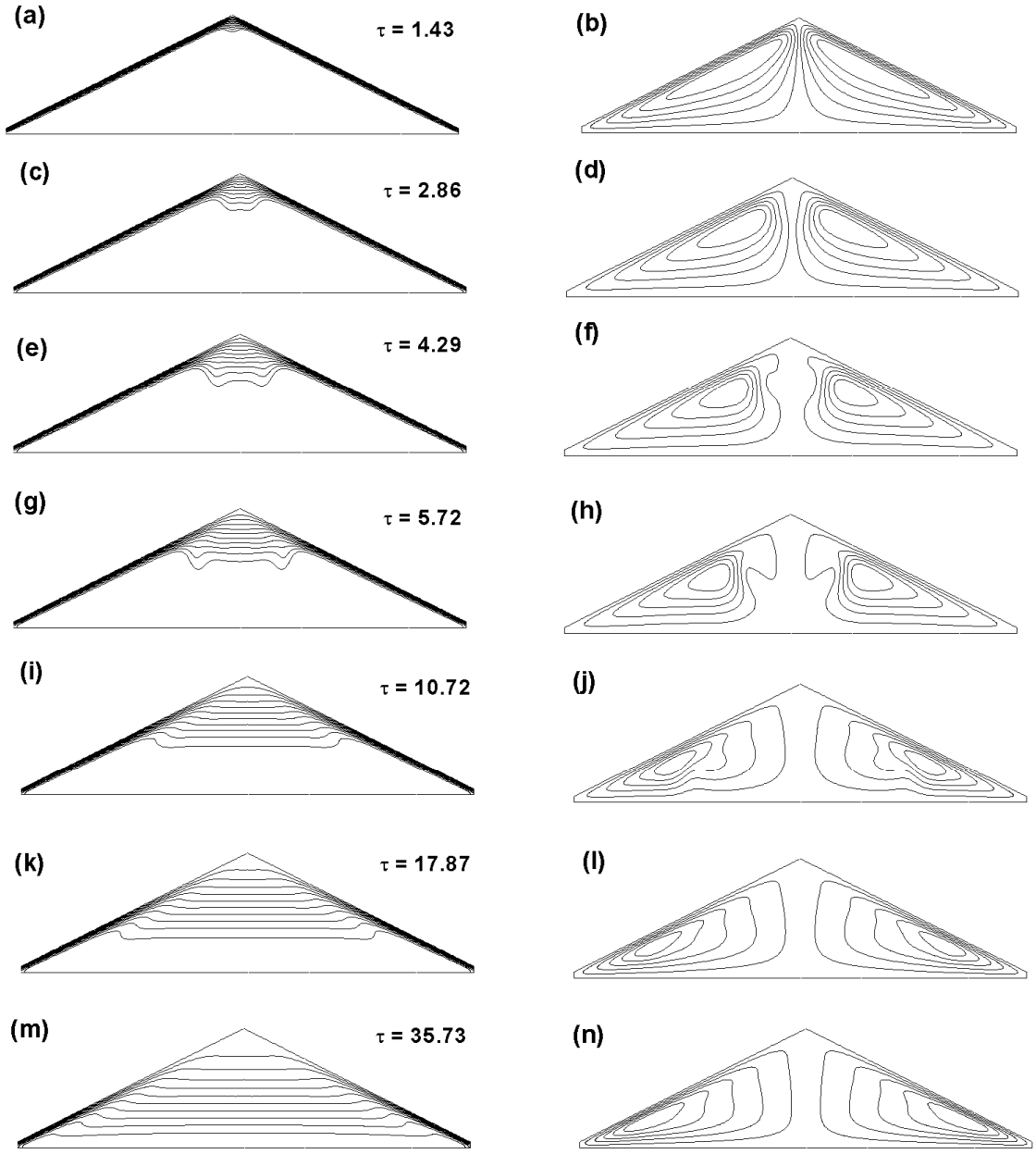

Fig. 2. Numerically simulated temperature contours (left) and stream functions (right) at of the boundary-layer development at $Ra = 10^7$, $Pr = 10$ and $A = 0.5$, where τ is the time normalised by h/U_0.

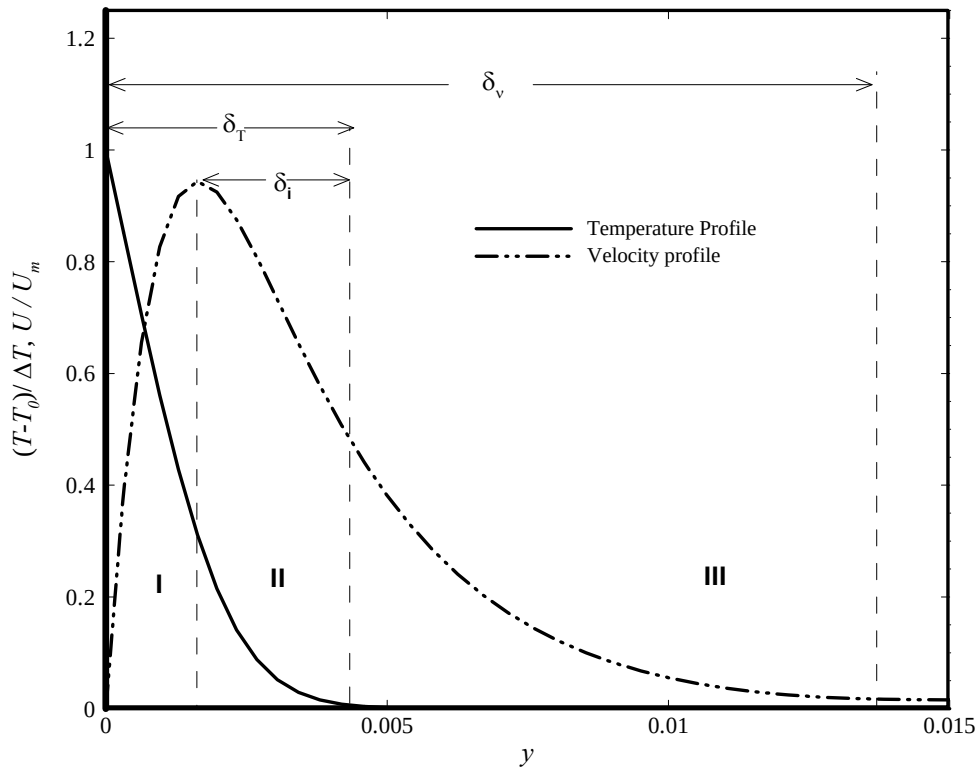

Fig. 3. A schematic of the temperature and velocity profiles normal to one of the inclined walls at its mid point.

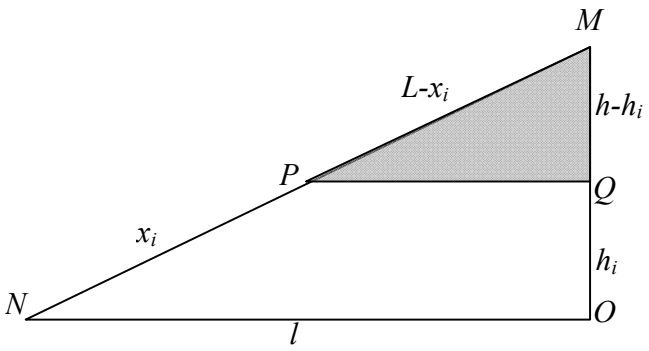

Fig. 4. Schematic of heating-up process for sudden heating.

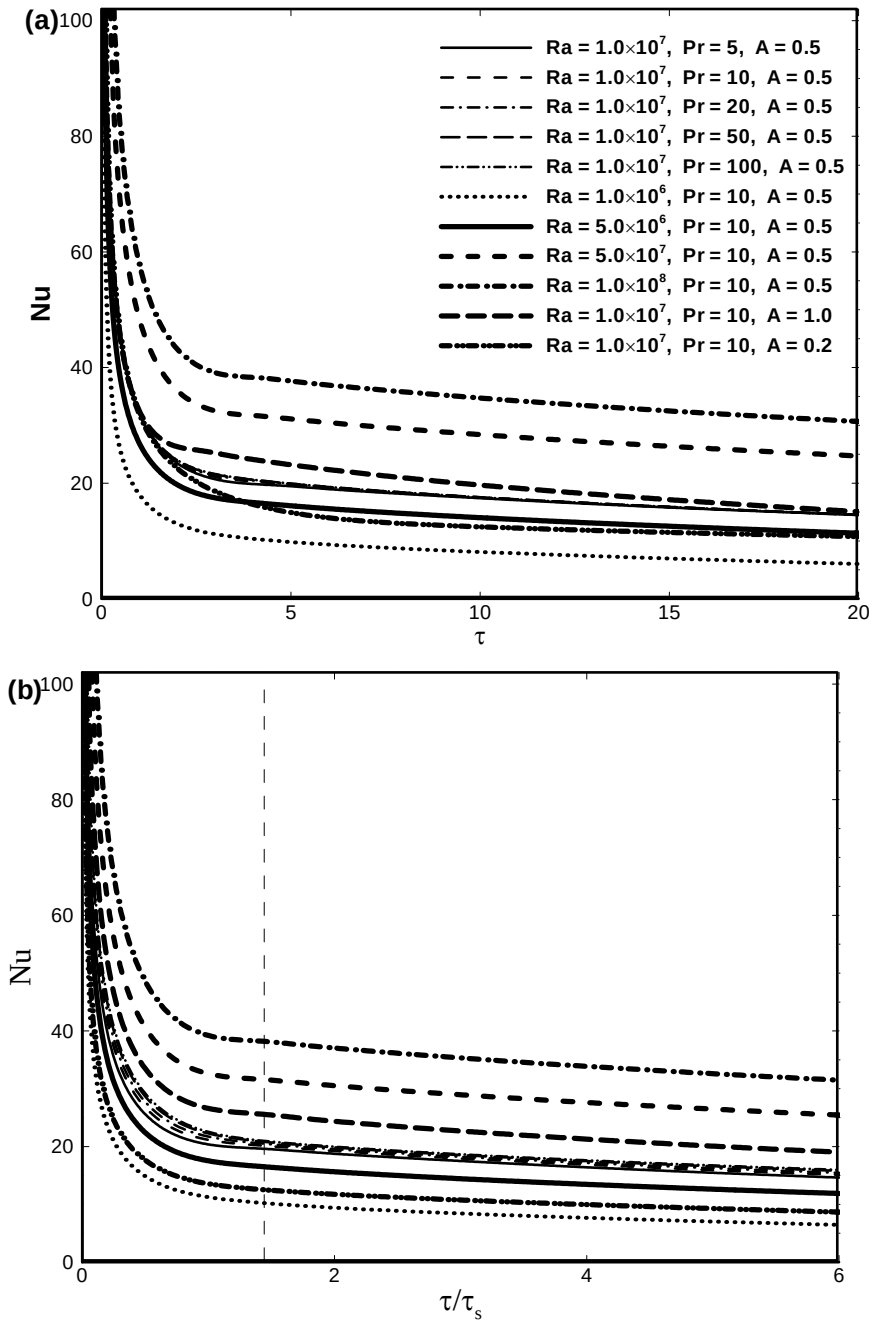

Figure 5 Nusselt number canculated on the heated plate for all cases considered: (a) raw data (b) *Nu* plotted against τ/τ_s.

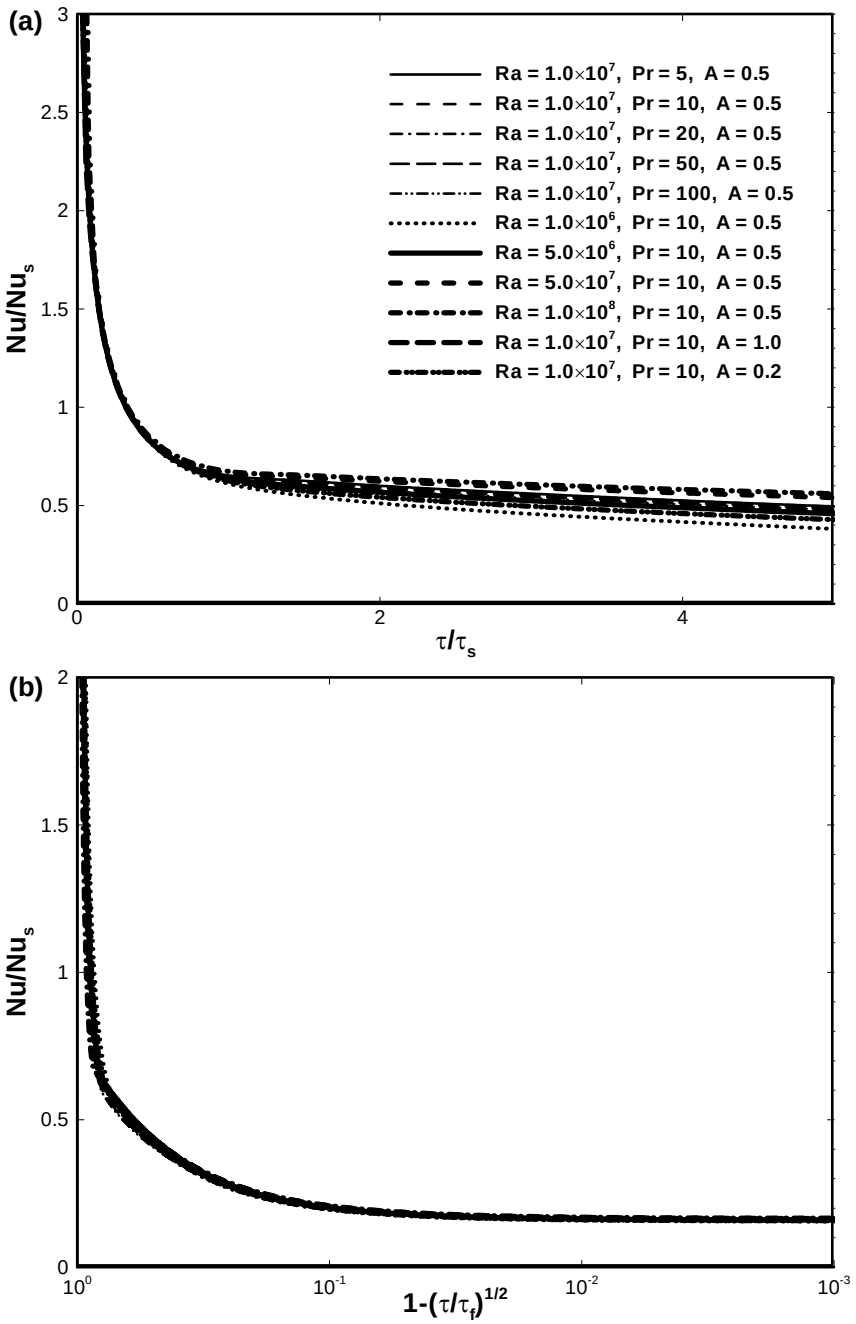

Figure 6 Nusselt number canculated on the heated plate for all cases considered: (a) Nu/Nu_s plotted against τ/τ_s (b) Nu/Nu_s plotted against $1-(\tau/\tau_s)^{1/2}$.

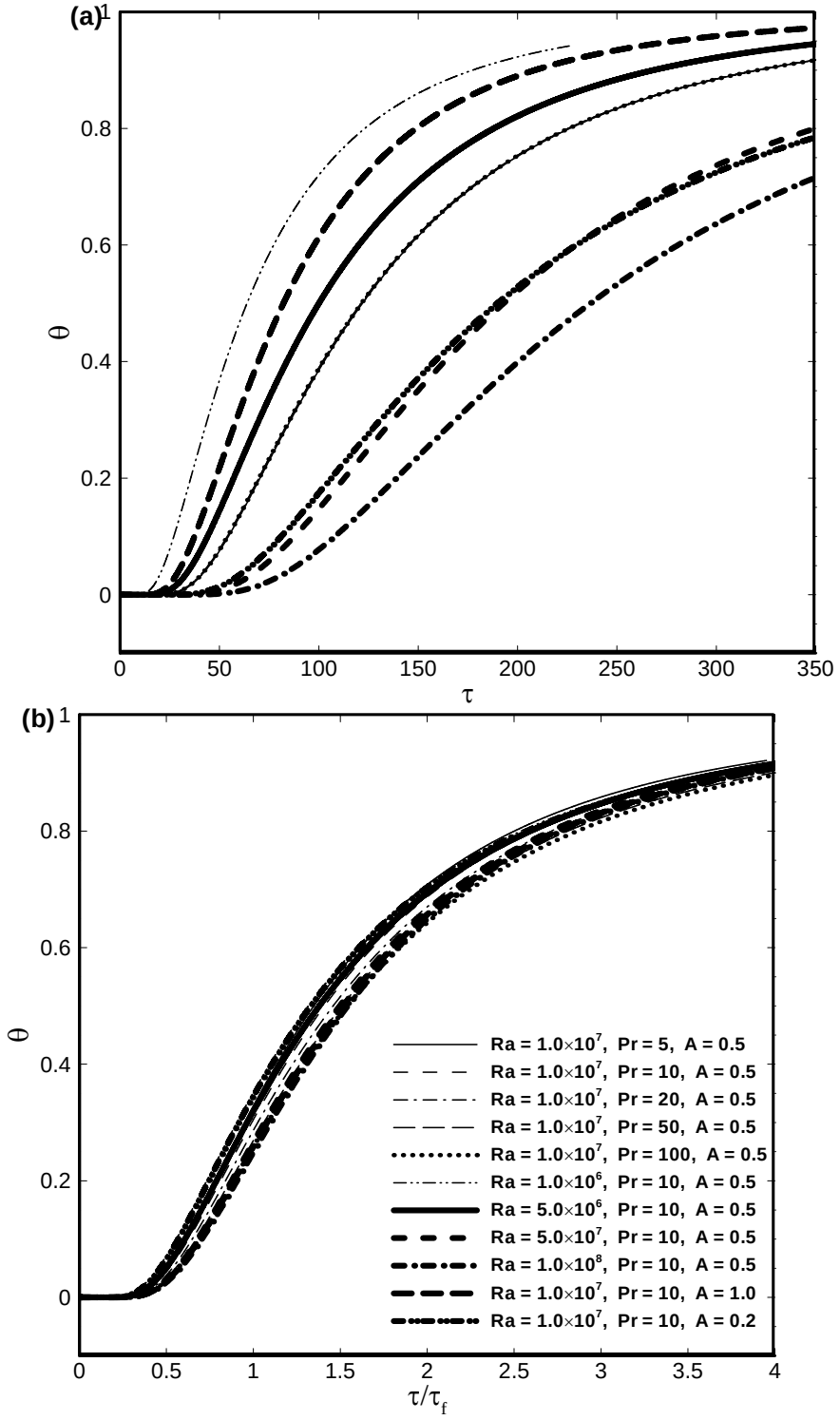

Figure 7 Time series of the maximum velocity parallel to the plate at x = 0.5 for all cases considered: (a) raw data and (b) θ plotted against $\tau[A^{1/2}(1+A^2)^{1/4}]/Ra^{1/4}(1+Pr^{-1/2})^{1/2}$.